Large Spin-Orbit Torque in a-Plane α-Fe_2O_3/Pt Bilayers

Igor Lyalin,[1] Hantao Zhang,[2] Justin Michel,[1] Daniel Russell,[1] Fengyuan Yang,[1] Ran Cheng,[2,3] and Roland K. Kawakami[1,*]

[1]*Department of Physics, The Ohio State University, Columbus, Ohio 43210, USA*
[2]*Department of Electrical and Computer Engineering, University of California, Riverside, California 92521, USA*
[3]*Department of Physics and Astronomy, University of California, Riverside, California 92521, USA*

(Received 25 June 2024; revised 13 August 2024; accepted 2 January 2025; published 12 February 2025)

Realization of efficient spin-orbit torque switching of the Néel vector in insulating antiferromagnets is a challenge, often complicated by spurious effects. Quantifying the spin-orbit torques in antiferromagnet or heavy metal heterostructures is an important first step toward this goal. Here, we employ magneto-optic techniques to study dampinglike spin-orbit torque (DL-SOT) in a-plane α-Fe_2O_3 (hematite) with a Pt spin-orbit overlayer. We find that the DL-SOT efficiency is 2 orders of magnitude larger than reported in c- and r-plane hematite/Pt using harmonic Hall techniques. The large magnitude of DL-SOT is supported by direct imaging of current-induced motion of antiferromagnetic domains that happens at moderate current densities. Our study introduces a new method for quantifying spin-orbit torque in antiferromagnets with a small canted moment and identifies a-plane α-Fe_2O_3 as a promising candidate to realize efficient SOT switching.

DOI: 10.1103/PhysRevLett.134.066701

Antiferromagnets (AFMs) display fast spin dynamics, produce no stray fields, and are robust against magnetic fields due to their vanishing magnetization. Thus, in principle, they can offer faster and denser magnetic memory than spintronic devices based on conventional ferromagnetic (FM) materials [1–3]. Efficient electrical control of antiferromagnetic order is one of the holy grails of antiferromagnetic spintronics. Spin-orbit torque (SOT) is an efficient way to manipulate magnetic order in ferromagnets [4–7]; however, the effects of SOT on antiferromagnets are less studied. In insulating AFM/heavy-metal (HM) bilayers, SOT switching is often complicated by spurious thermal effects arising from large electrical currents that are needed for the switching [8–12]. Therefore, developing alternative methods for characterizing the SOT in AFM/HM bilayers is an important step toward understanding SOT physics in these materials and realizing efficient electrical control. The current-modulated magneto-optic Kerr effect (MOKE) is a powerful technique for characterizing SOT [13,14]. Although this technique has been extensively applied to FMs [13–17], its application to SOT in AFMs has been mostly unexplored.

In this Letter, we report large dampinglike SOT in antiferromagnetic a-plane α-Fe_2O_3/Pt as characterized by current-modulated MOKE. We find that the DL-SOT efficiency in a-plane hematite/Pt bilayers is 2 orders of magnitude larger than reported in c-plane and r-plane samples [18,19]. In addition, we use MOKE microscopy to directly observe current-induced motion of AFM domains at moderate current densities, which corroborates the large magnitude of the DL-SOT. Thus, our study identifies a-plane α-Fe_2O_3 as a promising candidate to realize efficient SOT switching and calls for the development of hematite thin films with a-plane orientation.

The scientific results are enabled by significant technical advances needed for quantifying DL-SOT by magneto-optic methods. First, to properly analyze the current-modulated MOKE data, we develop a model that accounts for the antiferromagnetic nature of α-Fe_2O_3, including the Dzyaloshinskii-Moriya interaction (DMI) that generates a small canted moment. This canted moment facilitates the magneto-optic detection and quantification of the spin-orbit torque applied to an antiferromagnet.

Second, the small magnitude of the canted moment renders existing methods for calibrating the MOKE signal [15] (based on response to Oersted fields) ineffective. Therefore, we develop an alternative method for converting from MOKE units in radians to effective SOT field in Teslas (based on maximum Kerr ellipticity). We first demonstrate the validity of our modified approach by applying it to a well-studied material, thulium iron garnet $Tm_3Fe_5O_{12}$ (TmIG), an insulating ferrimagnet with perpendicular magnetic anisotropy.

TmIG/Pt films with 8/5 nm thickness are grown by off-axis magnetron sputtering [20] and patterned into a device geometry shown in Fig. 1(a) by a combination of photolithography and argon ion milling. The device channel width is 20 μm. We detect the out-of-plane magnetization, m_z, using the polar MOKE geometry and measuring

*Contact author: kawakami.15@osu.edu

 © 2025 American Physical Society

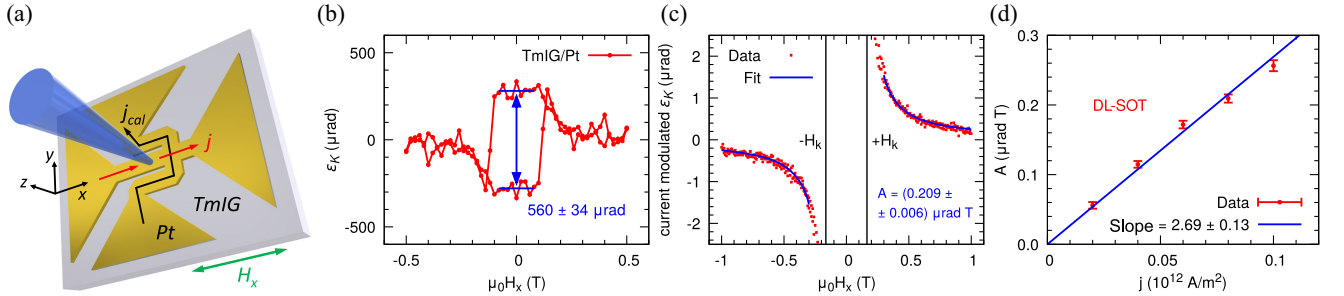

FIG. 1. TmIG/Pt (8/5 nm). (a) Schematics of current modulated MOKE experiment. (b) Kerr ellipticity (KE) as a function of magnetic field $\mu_0 H_x$ along hard axis of TmIG. (c) Current-modulated KE as a function of magnetic field $\mu_0 H_x$ for $j = 8 \times 10^{10}$ A/m^2. Here, the fitting parameter A is proportional to the dampinglike spin-orbit field H_{DL}. (d) Current-modulated KE as a function of current density j.

the Kerr ellipticity $\varepsilon_K \sim m_z$ of a linearly polarized laser light reflected from the sample. The laser beam is focused at the center of the device channel to ~5 μm spot size, the wavelength of the light is 400 nm. Figure 1(b) shows a Kerr ellipticity (KE) hysteresis loop with external magnetic field $\mu_0 H_x$ applied along hard axis of TmIG. When $\mu_0 H_x$ is larger than the anisotropy field $\mu_0 H_k$, the TmIG magnetization is along the x direction. With the current applied along the x axis as well, the spin Hall effect in the Pt layer generates spin current with polarization $\boldsymbol{\sigma}$ along the y axis. In this geometry, the effective dampinglike field $\boldsymbol{H}_{\mathrm{DL}} \sim [\boldsymbol{m} \times \boldsymbol{\sigma}] \sim [\hat{\boldsymbol{x}} \times \hat{\boldsymbol{y}}]$ results in a small tilt of magnetization toward the sample normal, thus inducing an out-of-plane component Δm_z. For a single domain state at $|H_x| > |H_k|$ and a small effective dampinglike field $H_{\mathrm{DL}} \ll |H_x - H_k|$, the out-of-plane current-induced magnetization can be written as [14]

$$\frac{\Delta m_z}{m} = \frac{\Delta \varepsilon_K^j}{\varepsilon_K^{\max}} = \frac{\mu_0 H_{\mathrm{DL}}}{|\mu_0 H_x - \mu_0 H_k|}, \tag{1}$$

where $\varepsilon_K^{\max}$ is the Kerr ellipticity that corresponds to the magnetization m being fully out of plane.

The current-modulated Kerr ellipticity $\Delta \varepsilon_K^j$ is detected using a combination of quarter-wave plate, half-wave plate, Wollaston prism, balanced photodetector, and lock-in amplifier at the frequency of the applied ac current. Figure 1(c) shows $\Delta \varepsilon_K^j$ as a function of magnetic field $\mu_0 H_x$ for a current density of $j = 8 \times 10^{10}$ A/m^2. Following Eq. (1), the data can be fitted using the expression $\Delta \varepsilon_K^j = A/|\mu_0 H_x - \mu_0 H_k|$ with two fitting parameters A and H_k, where $A = \varepsilon_K^{\max} \mu_0 H_{\mathrm{DL}}$. Measuring current-modulated KE at different current densities, we verify that $A \sim H_{\mathrm{DL}}$ scales linearly with j. This rules out contributions from thermal effects and agrees with the SOT origin of the measured signal [13]. The current density dependence is plotted in Fig. 1(d). Using the A/j slope normalized by $\varepsilon_K^{\max}$, extracted as a half of the hysteresis loop opening at $\mu_0 H_x = 0$ in Fig. 1(b), one can estimate the DL-SOT efficiency,

$$\frac{A}{j}\frac{1}{\varepsilon_K^{\max}} = \frac{\mu_0 H_{\mathrm{DL}}}{j} = \frac{\hbar}{2e}\frac{\xi_{\mathrm{DL}}}{M_s t_{\mathrm{FM}}}. \tag{2}$$

Using the measured values $A/j = 2.69 \pm 0.13$ μrad rad T per 10^{12} A/m^2, $\varepsilon_K^{\max} = 280 \pm 17$ μrad, and $t_{\mathrm{FM}} = 8$ nm along with $M_s = 110$ kA/m from the literature (saturation magnetization of TmIG [20]), we estimate the effective DL-SOT field and efficiency to be $\mu_0 H_{\mathrm{DL}}/j = 9.6 \pm 0.8$ mT per 10^{12} A/m^2 and $\xi_{\mathrm{DL}} = 0.026 \pm 0.002$, respectively. This agrees well with studies on insulating FM/HM bilayers, in which DL-SOT efficiency has been found to be smaller than in metallic FM/HM. The literature on TmIG/Pt reports values of 0.01–0.03 SOT efficiency [21,22]. We note that to correctly estimate $\varepsilon_K^{\max}$, the magnetic material should be in a single domain state within the laser spot size (at $\mu_0 H_x = 0$) or the out-of-plane $\mu_0 H_z$ hysteresis loop should be measured to extract $\varepsilon_K^{\max}$.

To further test the validity of our experimental approach, we compared our results to the method developed in Refs. [13,15], in which the DL-SOT field is calibrated against an Oersted field generated by a wire of known geometry. The current path for the calibration wire in our device is shown in Fig. 1(a) and is labeled as $\boldsymbol{j}_{\mathrm{cal}}$. Using this method, we find $\mu_0 H_{\mathrm{DL}}/j = 8.3 \pm 0.7$ mT per 10^{12} A/m^2, which within experimental errors agrees with the value estimated by the $\varepsilon_K^{\max}$ normalization method; see SM, Sec. S1 [23] for details.

Having verified that our modified approach is valid, we discuss the spin-orbit torque measurements in a-plane α-Fe_2O_3/Pt (bulk/5 nm). A commercial bulk crystal with dimensions $5 \times 5 \times 1$ mm and $(11\bar{2}0)$ cut (a-plane) is purchased from MTI Corporation. A 5 nm Pt is deposited by magnetron sputtering at room temperature. The geometry of the current-modulated MOKE experiment, Fig. 2(a), is similar to the measurements on TmIG/Pt, with a difference that now the spin-flop field, H_{sf}, is needed to align the magnetization along the x direction, instead of the anisotropy field H_k. Figure 2(b) illustrates the difference between the action of dampinglike spin-orbit torque on ferrimagnetic TmIG and antiferromagnetic α-Fe_2O_3. A charge current through the Pt layer is applied along the

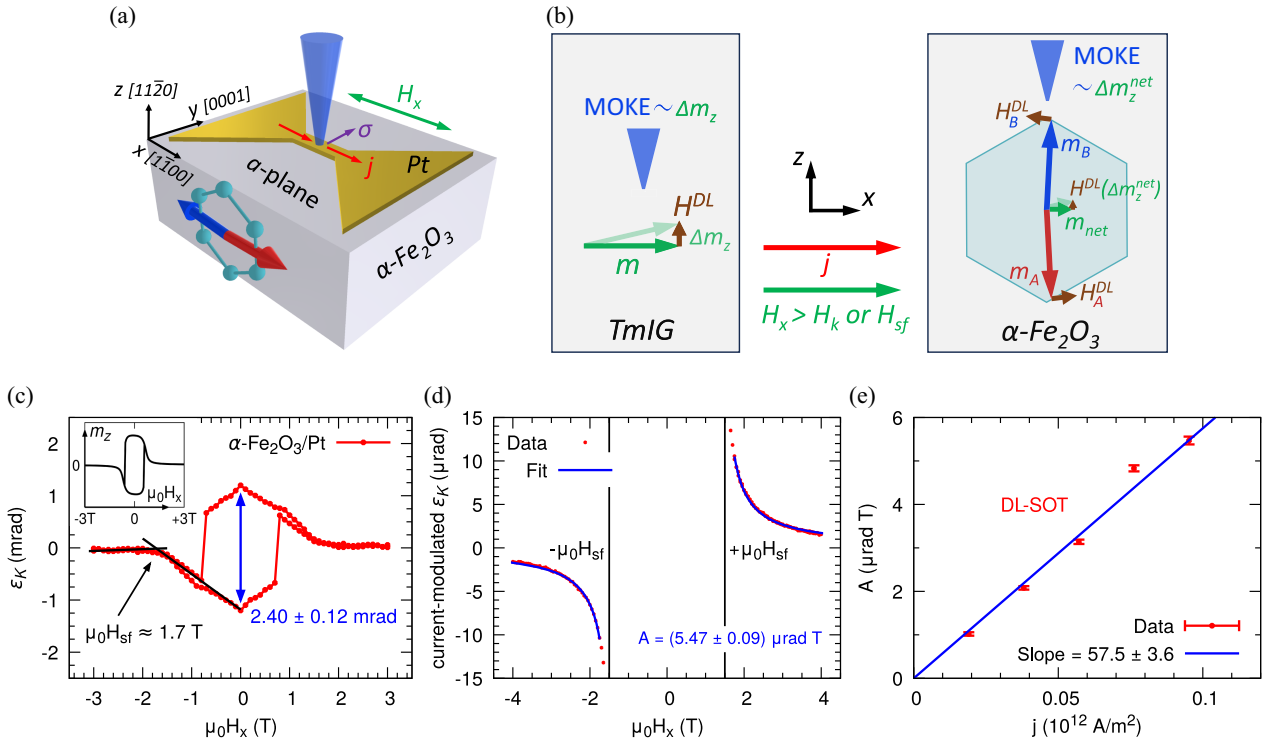

FIG. 2. a-plane α-Fe_2O_3/Pt (bulk/5 nm). (a) Schematics of the current modulated MOKE experiment. (b) Schematics of DL-SOT in TmIG vs α-Fe_2O_3. (c) Kerr ellipticity as a function of magnetic field $\mu_0 H_x$ along the [1$\bar{1}$00] direction. The inset shows a simulated m_z vs $\mu_0 H_x$ loop. (d) Current-modulated KE as a function of magnetic field $\mu_0 H_x$ for $j = 9.5 \times 10^{10}$ A/m^2. The red dots are the experimental data, and the blue curve is a fit to the theoretical model, which yields a best-fit value of $A = 5.47$ μrad T, which is proportional to the dampinglike spin-orbit field H_{DL} (see text for the definition of A). (e) Fitting parameter A $(\sim H_{\mathrm{DL}})$ as a function of current density j.

[1$\bar{1}$00] direction [x axis in Fig. 2(a)] and as a result, the spin polarization $\boldsymbol{\sigma}$ is along [0001] (y axis). The effective dampinglike field acts on the magnetic moments of both sublattices: $\boldsymbol{H}_{\mathrm{DL}}^{A} \sim [\boldsymbol{m}_A \times \boldsymbol{\sigma}]$ and $\boldsymbol{H}_{\mathrm{DL}}^{B} \sim [\boldsymbol{m}_B \times \boldsymbol{\sigma}]$. The two torques act constructively to rotate the Néel vector and the canted magnetic moment ($\boldsymbol{m}_{\mathrm{net}}$) in the basal plane. For $|H_x| > |H_{\mathrm{sf}}|$, the $\boldsymbol{m}_{\mathrm{net}}$ is rotated out of the sample plane and the resultant out-of-plane component $\Delta m_z^{\mathrm{net}}$ can be detected by a current-modulated polar MOKE.

Kerr ellipticity as a function of magnetic field swept along [1$\bar{1}$00] direction (H_x) is plotted in Fig. 2(c). The KE signal due to the small canted moment in antiferromagnetic α-Fe_2O_3 is large, $\varepsilon_K^{\max} = 1.20 \pm 0.06$ mrad, roughly 4–5 times larger than for ferrimagnetic TmIG. This could be explained by the larger thickness of α-Fe_2O_3 vs TmIG (bulk vs 8 nm) and the difference in magneto-optic coefficients at 400 nm. The large magnitude of the MOKE signal facilitates the magneto-optical detection of the spin-orbit torque. The spin-flop field can be estimated from the KE hysteresis loop along [1$\bar{1}$00], as shown in Fig. 2(c), $\mu_0 H_{\mathrm{sf}} \approx 1.7$ T, which agrees with an estimation based on spin Hall magnetoresistance measurements, $\mu_0 H_{\mathrm{sf}} \approx 1.5$ T; see Supplemental Material [23], Sec. S2, for details.

We also simulate m_z vs $\mu_0 H_x$ numerically (see SM, Sec. S3, for details). Setting the exchange field $\mu_0 H_E = 900$ T, anisotropy field in the basal plane $\mu_0 H_K = 6 \times 10^{-4}$ T, DMI field $\mu_0 H_D = 2.5$ T, which are close to values reported in the literature [26–30], and a misalignment angle of 3° between the external magnetic field and the [1$\bar{1}$00] crystallographic direction, we are able to qualitatively reproduce the experimental data. The simulated hysteresis loop is shown in the inset of Fig. 2(c). We note that the polarity of the hysteresis loop is sensitive to the misalignment angle of the magnetic field. The sharp feature at $\mu_0 H_x = 0$ T in the experimental loop is likely from multidomain structure, which is not accounted for in the monodomain simulation.

Next, we quantify DL-SOT using current-modulated Kerr ellipticity as a function of magnetic field $\mu_0 H_x$, as shown in Fig. 2(d). The MOKE signal from the canted moment behaves similarly to the case of a ferromagnetic or ferrimagnetic material with perpendicular magnetic anisotropy [see Fig. 1(c)]. However, the antiferromagnetic case is more complex due to the competing exchange, DMI, and anisotropy energies. We show that for $|H_x| > |H_{\mathrm{sf}}|$, when the sample is in a single domain state, the data can be fitted using an expression (see SM, Sec. S3),

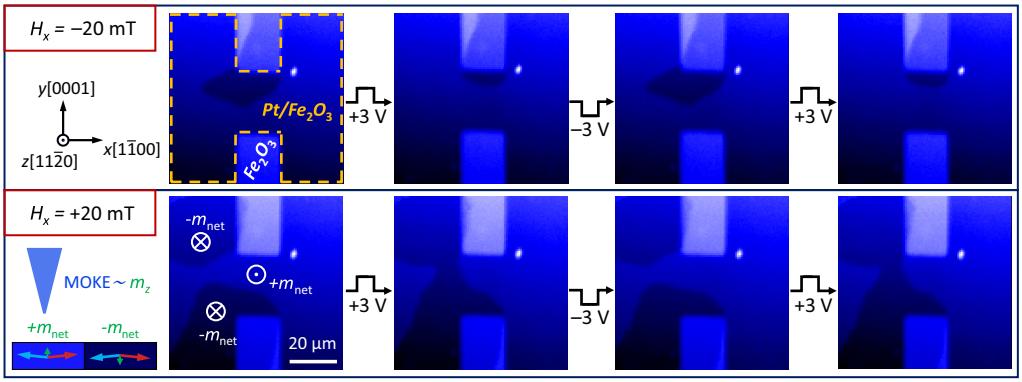

FIG. 3. MOKE microscopy maps of an α-Fe_2O_3/Pt device revealing current-induced domain motion. The 3 V amplitude of voltage pulses corresponds to $j = 2.4 \times 10^{11}$ A/m^2 current density. The pulse duration is 10 μs. A white spot in the top right quadrant is due to a dust particle on the Pt surface.

$$\frac{\Delta m_z}{m} = \frac{\Delta \varepsilon_K^j}{\varepsilon_K^{\max}} = \frac{\mu_0 H_{\mathrm{DL}}}{\left|\mu_0 H_x - \mu_0 \frac{4 H_E H_K}{(H_x + H_D)}\right|}. \tag{3}$$

We fix $\mu_0 H_D$ to a value of 2.5 T as it is more established in the literature [26–30] and fit the current-modulated Kerr ellipticity data $\Delta\varepsilon_K^j(H_x)$ using two fitting parameters $A = \varepsilon_K^{\max}\mu_0 H_{\mathrm{DL}}$ and $B = \mu_0^2 H_E H_K$. The result of the fit is the blue curve in Fig. 2(d).

Next, we measure the current-modulated MOKE signal at different current densities and repeat the fitting procedure. As shown in Fig. 2(e), we observe that A scales linearly with current density j, consistent with the SOT origin of the MOKE signal. Similar to TmIG/Pt analysis, using the measured values of the slope $A/j = 57.5 \pm 3.6$ μrad T per 10^{12} A/m^2 and $\varepsilon_K^{\max} = 1.20 \pm 0.06$ mrad, we can estimate the effective DL-SOT field. We find $\mu_0 H_{\mathrm{DL}}/j = 47.9 \pm 3.9$ mT per 10^{12} A/m^2. We note that the fitting is not too sensitive to the fixed value of the DMI field. Varying the $\mu_0 H_D$ value in the 1–10 T range changes the value of $\mu_0 H_{\mathrm{DL}}$ only by 20%.

The $\mu_0 H_{\mathrm{DL}}/j$ value is 2 orders of magnitude larger than effective DL-SOT field reported in c-plane and r-plane hematite using the harmonic Hall technique [18,19] and larger than values for thick metallic FM/Pt bilayers [4]. We note that we study a bulk sample and that even larger H_{DL} should be expected for thin films. We also point out that in c-plane α-Fe_2O_3, $\boldsymbol{H}_{\mathrm{DL}}$ points along the c axis and thus it needs to overcome the strong easy-plane anisotropy in order to realize the switching. For r-plane orientation, this effect is mitigated, while for a-plane orientation, $\boldsymbol{H}_{\mathrm{DL}}$ fully lies within the easy plane, and consequently, its effect on the rotation of the Néel vector is maximized. Thus, a-plane α-Fe_2O_3/Pt might be a promising material system to realize efficient SOT switching of the Néel vector. To check that our results are robust to a different location on the sample, device geometry, and optical alignment, we reproduce results on a different α-Fe_2O_3/Pt device. The data on the other device are shown in the SM, Sec. S4. We find $\mu_0 H_{\mathrm{DL}}/j = 54.1 \pm 3.2$ mT per 10^{12} A/m^2, which agrees well with the result on the device shown in Fig. 2.

Finally, we utilize MOKE microscopy to directly image AFM domains in a-plane α-Fe_2O_3/Pt. Figure 3 shows polar MOKE maps of a 21 μm wide and 20 μm long device. Large, tens of micrometers in size, AFM domains with a canted moment $\boldsymbol{m}_{\mathrm{net}}$ along the $+z$ (light blue) and $-z$ (dark blue) directions are observed for small applied magnetic fields below the spin-flop transition (see SM, Sec. S5, for a discussion of the easy axis in the basal plane and additional magneto-optic measurements supporting the interpretation of the MOKE images). Using a small bias field, $\mu_0 H_x = \pm 20$ mT, we demonstrate a current-driven AFM domain motion. For $\mu_0 H_x = -20$ mT, a $-m_z$ domain in the center of the device reproducibly shrinks (expands) after a positive +3 V (negative −3 V) pulse that corresponds to a moderate current density of 2.4×10^{11} A/m^2. The duration of pulses is 10 μs. When the bias field is reversed to $\mu_0 H_x = -20$ mT, the polarity of the domain motion changes. Now, $a + m_z$ domain shrinks (expands) after a positive +3 V (negative −3 V) pulse. This behavior is fully consistent with a protocol for dampinglike SOT-driven domain motion in FM/HM bilayers [31]. The SOT-driven motion of AFM domain at moderate current densities supports the large measured value of DL-SOT efficiency. For comparison, current densities of 2×10^{12} A/m^2 are needed for partial switching of domains in c-plane α-Fe_2O_3/Pt films [32], which is attributed to a combination of SOT and thermal effects. In addition, we note that for many AFMs, synchrotron facilities are required for direct imaging of AFM domains [9,12,32], whereas our results show that domains in a-plane α-Fe_2O_3 can be readily imaged by a tabletop technique.

It is theoretically argued that the dampinglike SOT, rather than the fieldlike one, is required to switch the Néel vector [1]. The magnitude of the dampinglike SOT

measured in our work is considerably larger compared to previous reports on α-Fe_2O_3/HM bilayers [18,19]. This is great news for the efficient electrical control of the AFM order, but it also raises a question about the origin of the enhanced torque. One possibility is that, in comparison with *c*-plane samples, in *a*-plane hematite, the DL-SOT is not suppressed by a large anisotropy along the *c* axis, making the SOT effect much larger. However, the SOT study on *r*-plane hematite [19] (with the sample plane in between the *c* and *a* planes) also found a small value of DL-SOT. Thus, while it is true that the DL-SOT effect is maximized for *a*-plane orientation, it is unlikely to account for the 100 times enhancement of DL-SOT in comparison with *r*-plane samples. Another possibility is related to the interface. It was proposed that a low spin-mixing conductance of the thin film α-Fe_2O_3/HM interface can explain a small magnitude of the dampinglike SOT [18,19]. Contrary to these works on thin films, a spin-pumping study on bulk *c*-plane α-Fe_2O_3/HM samples [30] estimated the spin-mixing conductance to be 2 orders of magnitude larger than those reported in other AFM/HM systems. Thus, a high spin-mixing conductance of the bulk α-Fe_2O_3 and Pt interface could account for the enhanced DL-SOT in our samples. This indicates that the quality of the thin films and bulk crystals could differ significantly. More studies are needed to systematically investigate the interface between α-Fe_2O_3 and a heavy metal in order to understand and maximize the SOT in this promising material system. We also note that hematite is predicted to be an altermagnet [33,34]. Similar to how spin current generation depends on crystallographic direction in metallic altermagnets [35,36], magnon spin current can be anisotropic [37]. This could potentially explain the difference in SOT for *a*-plane vs *c*- and *r*-plane samples. However, this is a speculation, and further studies would be needed to investigate it.

In conclusion, we utilized current-modulated MOKE to characterize spin-orbit torque in *a*-plane α-Fe_2O_3/Pt bilayers. We found that dampinglike SOT is 100 times larger than reported in *c*-plane and *r*-plane samples. Our study identifies *a*-plane α-Fe_2O_3 as a promising candidate to realize efficient SOT switching and calls for the development of thin films with an *a*-plane orientation.

Acknowledgments—This research was primarily supported (I. L., D. R., F. Y., R. K. K.) by the Center for Emergent Materials, an NSF MRSEC, under Grant No. DMR-2011876 and partially supported (J. M., F. Y.) by the Department of Energy, Office of Science, Basic Energy Sciences, under Award No. DE-SC0001304. R. C. and H. Z. were supported by the Air Force Office of Scientific Research under Grant No. FA9550-19-1-0307.

[1] V. Baltz, A. Manchon, M. Tsoi, T. Moriyama, T. Ono, and Y. Tserkovnyak, Antiferromagnetic spintronics, Rev. Mod. Phys. **90**, 015005 (2018).
[2] S. Fukami, V. O. Lorenz, and O. Gomonay, Antiferromagnetic spintronics, J. Appl. Phys. **128**, 070401 (2020).
[3] J. Han, R. Cheng, L. Liu, H. Ohno, and S. Fukami, Coherent antiferromagnetic spintronics, Nat. Mater. **22**, 684 (2023).
[4] L. Liu, T. Moriyama, D. C. Ralph, and R. A. Buhrman, Spin-torque ferromagnetic resonance induced by the spin Hall effect, Phys. Rev. Lett. **106**, 036601 (2011).
[5] I. M. Miron, K. Garello, G. Gaudin, P.-J. Zermatten, M. V. Costache, S. Auffret, S. Bandiera, B. Rodmacq, A. Schuhl, and P. Gambardella, Perpendicular switching of a single ferromagnetic layer induced by in-plane current injection, Nature (London) **476**, 189 (2011).
[6] L. Liu, C.-F. Pai, Y. Li, H. W. Tseng, D. C. Ralph, and R. A. Buhrman, Spin-torque switching with the giant spin Hall effect of tantalum, Science **336**, 555 (2012).
[7] A. Manchon, J. Železný, I. M. Miron, T. Jungwirth, J. Sinova, A. Thiaville, K. Garello, and P. Gambardella, Current-induced spin-orbit torques in ferromagnetic and antiferromagnetic systems, Rev. Mod. Phys. **91**, 035004 (2019).
[8] C. C. Chiang, S. Y. Huang, D. Qu, P. H. Wu, and C. L. Chien, Absence of evidence of electrical switching of the antiferromagnetic Néel vector, Phys. Rev. Lett. **123**, 227203 (2019).
[9] L. Baldrati, O. Gomonay, A. Ross, M. Filianina, R. Lebrun, R. Ramos, C. Leveille, F. Fuhrmann, T. R. Forrest, F. Maccherozzi, S. Valencia, F. Kronast, E. Saitoh, J. Sinova, and M. Kläui, Mechanism of Néel order switching in antiferromagnetic thin films revealed by magnetotransport and direct imaging, Phys. Rev. Lett. **123**, 177201 (2019).
[10] P. Zhang, J. Finley, T. Safi, and L. Liu, Quantitative study on current-induced effect in an antiferromagnet insulator/Pt bilayer film, Phys. Rev. Lett. **123**, 247206 (2019).
[11] A. Churikova, D. Bono, B. Neltner, A. Wittmann, L. Scipioni, A. Shepard, T. Newhouse-Illige, J. Greer, and G. S. D. Beach, Non-magnetic origin of spin Hall magnetoresistance-like signals in Pt films and epitaxial NiO/Pt bilayers, Appl. Phys. Lett. **116**, 022410 (2020).
[12] H. Meer, F. Schreiber, C. Schmitt, R. Ramos, E. Saitoh, O. Gomonay, J. Sinova, L. Baldrati, and M. Kläui, Direct imaging of current-induced antiferromagnetic switching revealing a pure thermomagnetoelastic switching mechanism in NiO, Nano Lett. **21**, 114 (2021).
[13] X. Fan, H. Celik, J. Wu, C. Ni, K.-J. Lee, V. O. Lorenz, and J. Q. Xiao, Quantifying interface and bulk contributions to spin–orbit torque in magnetic bilayers, Nat. Commun. **5**, 3042 (2014).
[14] X. Fan, A. R. Mellnik, W. Wang, N. Reynolds, T. Wang, H. Celik, V. O. Lorenz, D. C. Ralph, and J. Q. Xiao, All-optical vector measurement of spin-orbit-induced torques using both polar and quadratic magneto-optic Kerr effects, Appl. Phys. Lett. **109**, 122406 (2016).
[15] W. Wang, T. Wang, V. P. Amin, Y. Wang, A. Radhakrishnan, A. Davidson, S. R. Allen, T. J. Silva, H. Ohldag, D. Balzar, B. L. Zink, P. M. Haney, J. Q. Xiao, D. G. Cahill, V. O. Lorenz, and X. Fan, Anomalous spin–orbit torques in magnetic single-layer films, Nat. Nanotechnol. **14**, 819 (2019).
[16] I. Lyalin, S. Cheng, and R. K. Kawakami, Spin–orbit torque in bilayers of kagome ferromagnet Fe_3Sn_2 and Pt, Nano Lett. **21**, 6975 (2021).

[17] N. L. L. Pham, K.-H. Ko, and G.-M. Choi, Ferromagnetic material dependence of spin–orbit torque in PtMn/ferromagnet bilayer, Appl. Phys. Lett. **123**, 162402 (2023).
[18] E. Cogulu, H. Zhang, N. N. Statuto, Y. Cheng, F. Yang, R. Cheng, and A. D. Kent, Quantifying spin-orbit torques in antiferromagnet–heavy-metal heterostructures, Phys. Rev. Lett. **128**, 247204 (2022).
[19] P. Zhang, C.-T. Chou, H. Yun, B. C. McGoldrick, J. T. Hou, K. A. Mkhoyan, and L. Liu, Control of Néel vector with spin-orbit torques in an antiferromagnetic insulator with tilted easy plane, Phys. Rev. Lett. **129**, 017203 (2022).
[20] A. S. Ahmed, A. J. Lee, N. Bagués, B. A. McCullian, A. M. A. Thabt, A. Perrine, P.-K. Wu, J. R. Rowland, M. Randeria, P. C. Hammel, D. W. McComb, and F. Yang, Spin-Hall topological Hall effect in highly tunable Pt/ferromagnetic-insulator bilayers, Nano Lett. **19**, 5683 (2019).
[21] C. O. Avci, A. Quindeau, C.-F. Pai, M. Mann, L. Caretta, A. S. Tang, M. C. Onbasli, C. A. Ross, and G. S. D. Beach, Current-induced switching in a magnetic insulator, Nat. Mater. **16**, 309 (2017).
[22] T. Li, L. Liu, X. Li, X. Zhao, H. An, and K. Ando, Giant orbital-to-spin conversion for efficient current-induced magnetization switching of ferrimagnetic insulator, Nano Lett. **23**, 7174 (2023).
[23] See Supplemental Material at http://link.aps.org/supplemental/10.1103/PhysRevLett.134.066701 for details on the calibration of MOKE signal by Oersted field in TmIG/Pt, the additional magnetic circular dichroism and angular-dependent magnetoresistance measurements of α-Fe_2O_3/Pt, current-modulated MOKE measurements of another α-Fe_2O_3 device, and theoretical derivation of the fitting formula, which includes Refs. [24,25].
[24] H. Zhang and R. Cheng, Theory of harmonic Hall responses of spin-torque driven antiferromagnets, J. Magn. Magn. Mater. **556**, 169362 (2022).
[25] A. Qaiumzadeh, H. Skarsvåg, C. Holmqvist, and A. Brataas, Spin superfluidity in biaxial antiferromagnetic insulators, Phys. Rev. Lett. **118**, 137201 (2017).
[26] S. J. Williamson and S. Foner, Antiferromagnetic resonance in systems with Dzyaloshinsky-Moriya coupling; orientation dependence in α-Fe_2O_3, Phys. Rev. **136**, A1102 (1964).
[27] K. Mizushima and S. Iida, Effective in-plane anisotropy field in α-Fe_2O_3, J. Phys. Soc. Jpn. **21**, 1521 (1966).
[28] P. R. Elliston and G. J. Troup, Some antiferromagnetic resonance measurements in α-Fe_2O_3, J. Phys. C **1**, 169 (1968).
[29] R. Lebrun, A. Ross, O. Gomonay, S. A. Bender, L. Baldrati, F. Kronast, A. Qaiumzadeh, J. Sinova, A. Brataas, R. A. Duine, and M. Kläui, Anisotropies and magnetic phase transitions in insulating antiferromagnets determined by a Spin-Hall magnetoresistance probe, Commun. Phys. **2**, 50 (2019).
[30] H. Wang, Y. Xiao, M. Guo, E. Lee-Wong, G. Q. Yan, R. Cheng, and C. R. Du, Spin pumping of an easy-plane antiferromagnet enhanced by Dzyaloshinskii–Moriya interaction, Phys. Rev. Lett. **127**, 117202 (2021).
[31] S. Vélez, J. Schaab, M. S. Wörnle, M. Müller, E. Gradauskaite, P. Welter, C. Gutgsell, C. Nistor, C. L. Degen, M. Trassin, M. Fiebig, and P. Gambardella, High-speed domain wall racetracks in a magnetic insulator, Nat. Commun. **10**, 4750 (2019).
[32] E. Cogulu, N. N. Statuto, Y. Cheng, F. Yang, R. V. Chopdekar, H. Ohldag, and A. D. Kent, Direct imaging of electrical switching of antiferromagnetic Néel order in α-Fe_2O_3 epitaxial films, Phys. Rev. B **103**, L100405 (2021).
[33] L. Šmejkal, J. Sinova, and T. Jungwirth, Beyond conventional ferromagnetism and antiferromagnetism: A phase with nonrelativistic spin and crystal rotation symmetry, Phys. Rev. X **12**, 031042 (2022).
[34] L. Šmejkal, J. Sinova, and T. Jungwirth, Emerging research landscape of altermagnetism, Phys. Rev. X **12**, 040501 (2022).
[35] A. Bose, N. J. Schreiber, R. Jain, D.-F. Shao, H. P. Nair, J. Sun, X. S. Zhang, D. A. Muller, E. Y. Tsymbal, D. G. Schlom, and D. C. Ralph, Tilted spin current generated by the collinear antiferromagnet ruthenium dioxide, Nat. Electron. **5**, 267 (2022).
[36] Z. Feng, X. Zhou, L. Šmejkal, L. Wu, Z. Zhu, H. Guo, R. González-Hernández, X. Wang, H. Yan, P. Qin, X. Zhang, H. Wu, H. Chen, Z. Meng, L. Liu, Z. Xia, J. Sinova, T. Jungwirth, and Z. Liu, An anomalous Hall effect in altermagnetic ruthenium dioxide, Nat. Electron. **5**, 735 (2022).
[37] L. Šmejkal, A. Marmodoro, K.-H. Ahn, R. González-Hernández, I. Turek, S. Mankovsky, H. Ebert, S. W. D'Souza, O. Sipr, J. Sinova, and T. Jungwirth, Chiral magnons in altermagnetic RuO_2, Phys. Rev. Lett. **131**, 256703 (2023).